ACADEMIC PRESS

Available online at www.sciencedirect.com
SCIENCE DIRECT®

Journal of Catalysis 216 (2003) 461–467

JOURNAL OF CATALYSIS

www.elsevier.com/locate/jcat

Reactive oxygen species in epoxidation reactions over titanosilicate molecular sieves

Vasudev N. Shetti, P. Manikandan, D. Srinivas, and P. Ratnasamy *

National Chemical Laboratory, Pune 411 008, India

Received 9 July 2002; revised 19 August 2002; accepted 26 August 2002

Abstract

In an attempt to rationalize the differences in the catalytic behavior of titanosilicate molecular sieves when using H_2O_2 (TS-1, TiMCM-41) versus $H_2 + O_2$ (Pd–TS-1) as oxidant, the Ti(IV)–superoxo and hydroperoxo/peroxo species formed in situ during the oxidation reactions were investigated by electron paramagnetic resonance (EPR) and diffuse reflectance UV–visible spectroscopies. Two types of superoxo species, A and B, were identified in TS-1; only the latter species was detected in TiMCM-41. EPR has provided evidence, for the first time, for the in situ generation of similar oxo species in reactions using $H_2 + O_2$ instead of H_2O_2. The Ti sites adjacent to Pd ions (in Pd–TS-1) behave differently magnetically than the other Ti ions, generating a greater variety of superoxo species (A′, A″, A, B′, B, and C) and corresponding reaction products. Pd enhances the reducibility of Ti and promotes formation of these oxo species at lower temperatures ($\sim$323 K). The epoxide selectivity in the oxidation of allyl alcohol over Pd–TS-1 is higher when using ($H_2 + O_2$) than when using H_2O_2. In all cases, type A species predominantly catalyze epoxidations while type B favor the hydroxylations. The selectivity for epoxidation (vis-à-vis allylic oxidation) over these catalysts can be enhanced by controlling the type of Ti–oxo species formed in situ during the oxidation process by a suitable combination of catalyst, oxidant, solvent, and temperature.

Keywords: Titanosilicates; TS-1; TiMCM-41; Reactive oxygen species; Ti(IV)–superoxide; Ti(IV)–hydroperoxide; Epoxidation of allyl alcohol; Oxidation with H_2O_2 and $H_2 + O_2$; EPR; Diffused reflectance UV–visible spectroscopy

1. Introduction

Titanosilicate molecular sieves, especially TS-1, have been widely studied for the selective oxidation of a variety of organic substrates, using aqueous H_2O_2 [1,2]. They were one of the earliest classes of molecular sieves containing a transition metal cation, Ti^{4+}, in framework positions and possessing remarkable activity and selectivity for partial hydrocarbon oxidation by H_2O_2. Molecular sieves containing a redox metal cation in framework positions have an enormous potential in shape-selective oxidation–reduction reactions, similar to the predominant role of their aluminosilicate analogs. However, compared to the enormous amount of literature on the structure and dynamics of the acidic, active sites (both Brønsted and Lewis type) in aluminosilicate zeolites, our knowledge of the reactive oxo intermediates over these titanosilicates is inadequate. IR spectroscopic studies [3] of TS-1 identified TiOOH (η^1) and Ti($O_2^{-\bullet}$) species in the presence of H_2O_2. Sankar et al. [4], using EXAFS measurements and DFT calculations, have claimed the existence of a bidentate (side on) peroxo species on Ti-grafted MCM-41. On the other hand, a bidentate hydroperoxo species (Ti–OOH (η^2)) had also been claimed [5] to be the reactive intermediate. Clarification and confirmation of the identity and role of oxo species generated on the surface of these interesting classes of materials will, we hope, enable the design and synthesis of tailor-made oxidation catalysts. As happened in the case of acidic aluminosilicate molecular sieves, oxidation reactions can then be investigated and put on more quantitative lines.

In spite of two decades of significant progress there are still many unresolved issues and challenges in this field. For example, why is TS-1 more chemoselective than Ti-beta and TiMCM-41 [6,7] even though Ti^{4+} ions are isolated and in tetrahedral locations in all of them? An understanding of this problem might lead to the development of efficient large-pore titanium silicate molecular sieves more active than the medium-pore TS-1 in the selective oxidation of large

* Corresponding author.
E-mail address: prs@ems.ncl.res.in (P. Ratnasamy).

0021-9517/03/$ – see front matter
doi:10.1016/S0021-9517(02)00119-7

molecules of interest to the fine-chemicals industry. Again, even though attempts have been made to replace aqueous H_2O_2 with a mixture of H_2 and O_2 in the presence of metals such as Pd, Pt, Au, and soforth [8–14], the observed catalytic activities are much lower. But selectivities of 99% for propylene oxide formation from propylene were observed by Haruta and co-workers [13] over Au-containing catalysts. In a preliminary study [15] we showed that reactive oxygen species (superoxides, hydroperoxides, and peroxides of Ti) generated during the oxidation process may influence the activity and selectivity of the titanosilicate molecular sieves.

In the present paper, we report a comprehensive investigation of such species formed in the presence of aqueous H_2O_2 (HP), urea–H_2O_2 adduct (UHP), and ($H_2 + O_2$) over TS-1, TiMCM-41, and Pd–TS-1 during the selective oxidation of allyl alcohol. Electron paramagnetic resonance (EPR) and diffuse reflectance UV–visible (DRUV–visible) spectroscopic techniques have been utilized to probe the structure and estimate the surface concentration of these oxygen species. The results lead to a better understanding and control of the catalytic behavior of these redox molecular sieves of great potential in the fine-chemicals industry.

2. Experimental

2.1. Sample preparation

TS-1 and TiMCM-41 were prepared according to reported procedures [15,16]. In the preparation of Pd(n)–TS-1 (n refers to the Pd content in weight percent) [9], an aqueous solution (15 ml) containing the required amounts of $[Pd(NH_3)_4]Cl_2 \cdot H_2O$ or $Pd(CH_3COO)_2$ (Aldrich) was added to TS-1 (3 g) taken in a 50-ml round-bottom flask. The slurry was stirred at 353 K for 20–24 h under N_2 atmosphere. The contents were then dried over a rotavapor (338 K) and then in a vacuum oven (348 K) for 15 h. The resultant solids were heated in nitrogen flow at 423 K for 2 h. Pt(0.015)–TS-1 was prepared similarly, except that $[Pt(NH_3)_4]Cl_2 \cdot H_2O$ was used. Both the Pd(n)–TS-1 and the Pt(0.015)–Pd(1)–TS-1 samples were grayish in color.

The urea–H_2O_2 adduct (UHP) was prepared by mixing equimolar quantities of urea and H_2O_2 (30%, SD Fine-Chem Ltd., India) and then stored in a dessicator.

2.2. Characterization procedures

TS-1 and TiMCM-41 were characterized by X-ray diffraction (Rigaku Miniflex XRD), wavelength dispersive X-ray fluorescence (Rigaku 3070 E XRF), and BET surface area measurements (Coulter 100) [15]. EPR spectra were recorded on a Bruker EMX spectrometer operating at X-band frequency and 100-kHz field modulation. Measurements at variable temperatures were done using a Bruker BVT 3000 temperature controller. Diffuse reflectance UV–visible (DRUV–visible) spectra were recorded with a Shimadzu (UV-2550) spectrophotometer. The titanosilicate samples were sprayed with a known quantity of a solvent/HP or mixed with UHP before the DRUV–visible spectra were recorded. EPR and DRUV–visible spectral simulations were done using the Bruker Simfonia and WINEPR software packages, respectively.

2.3. Sample treatments

A known quantity of titanosilicate (40 mg) was taken in 4.5-mm-o.d. Suprasil quartz EPR tubes. HP (50%, 0.1 ml) was added to it in amounts adequate enough to wet the solid completely. In the experiments on solvent effects, the titanosilicate samples were initially activated at 373 K in static air, cooled to 298 K, and then soaked in the desired solvent (0.4 ml). HP was next added and the EPR spectra were recorded.

In the experiments with UHP, 50 mg of titanosilicate was physically mixed (without grinding) with 100 mg of UHP. In the experiments involving solvents, this mixture was then exposed to solvent vapor (water, methanol, acetone, and acetonitrile) for 5–15 min before the spectra were recorded.

In the experiments with $H_2 + O_2$, the titanosilicates (40 mg) were initially evacuated at 423 K, for 2 h. Then the samples were reacted with dry hydrogen (20 ml/min), at 323–343 K, for 4 h and subsequently with molecular oxygen (20 ml/min) for 15 min. The sample temperature was quenched to 80 K and the EPR spectra were recorded.

2.4. Epoxidation of allyl alcohol

In a typical batch reaction, 100 mg of the catalyst, 10 g of acetone, and 0.5 g of AA were taken in a 50-ml double-necked round-bottom flask fitted with a water-cooled condenser. To this, HP (0.9 ml) was added. The reaction was carried out at 333 K, while being stirred, for 8 h. The products were analyzed by a gas chromatograph (CHROMPACK CP 9001; with a 50-m-long, 0.32-mm-i.d., and 0.3-μm-thick Hewlett–Packard fused silica capillary column) and a GC–MS (Shimadzu, QP-5000; with a 30-m-long, 0.25-mm-i.d., and 0.25-μm-thick capillary column DB-1). In the reactions with $H_2 + O_2$, 100 mg of the reduced catalyst, 5 g of acetone, 5 g of isopropanol, and 0.5 g of AA were taken in a double-necked round-bottom flask. The reactions were conducted at 333 K, for 8 h, while contacting with O_2 (20 ml/min).

3. Results and discussion

3.1. Physicochemical characterization

The crystallinity and phase purity of the titanosilicates were confirmed from the XRD patterns. The Si/Ti ratio (XRF) in TS-1 and TiMCM-41 were estimated to be 36 and 46, respectively. Their BET surface areas were 400 and 963 m^2/g, respectively. The pore diameter of TiMCM-41

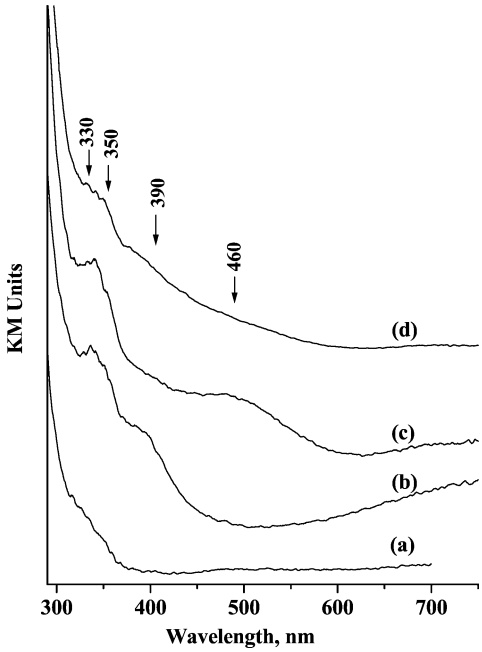

Fig. 1. DRUV–visible spectra (in Kubelka–Munk units) of (a) TS-1, (b) Pd(0.5)–TS-1 (before reduction), (c) Pd(2)–TS-1 (before reduction), and (d) Pd(2)–TS-1 (after reduction).

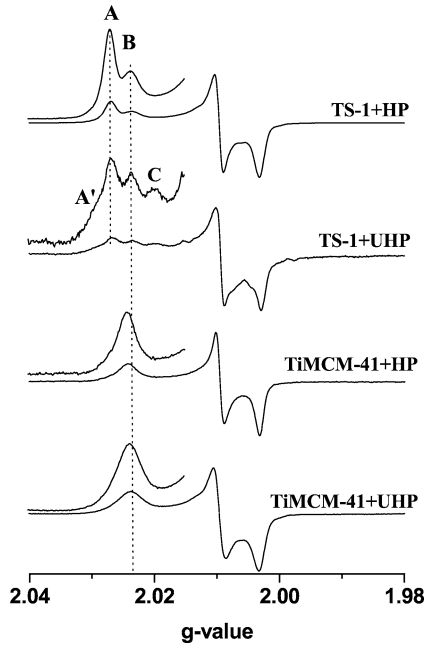

Fig. 2. EPR spectra of $Ti(O_2^{-\bullet})$ in TS-1 and TiMCM-41 in contact with H_2O_2 (HP) and urea–H_2O_2 (UHP). For clarity, the g_z region is shown at higher spectral gain. Signals corresponding to different $Ti(O_2^{-\bullet})$ species (A′, A, B, and C) are indicated.

was 30 Å. DRUV–visible spectra showed the O → Ti charge transfer band at 208 and 215 nm in TS-1 and TiMCM-41, respectively, indicating that the Ti^{4+} ions are isolated and isomorphously substituted in the silicate framework. Extraframework TiO_2 was negligible (< 0.01%; 335 nm).

In addition to the characteristic TS-1 band at 204 nm, Pd(0.5)–TS-1 showed charge transfer bands at 275, 350, and 392 nm, attributable to PdO_xCl_y or $PdO_x(OAc)_y$ species (Fig. 1). The broad background absorption in the region 450–850 nm is due to metallic Pd species. Samples with high Pd loadings showed an additional band, at 460 nm (curve c), due to a palladium oxide phase. In Pd(*n*)–TS-1, part of the Pd is in the +2 oxidation state and the remaining in the zero oxidation state. Similar observations were made by Meiers et al. [9,10] in the XPS of Pd–TS-1 samples. The samples were EPR silent, consistent with the +4 oxidation state of Ti in the silicate structures [15,17–19].

3.2. Interaction with HP, UHP, and ($H_2 + O_2$)

On interaction with HP and UHP the color of TS-1 and TiMCM-41 changed from white to yellow. The samples became paramagnetic, showing sharp EPR signals (Fig. 2) attributable to Ti(IV)–superoxo radical species ($Ti(O_2^{-\bullet})$) with one unpaired electron ($S = \frac{1}{2}$) [15,17–19]. Spectral simulations revealed two types of $Ti(O_2^{-\bullet})$ species, A and B (A being preponderant), in TS-1. Only species B was present in TiMCM-41. UHP, on interaction with TS-1, generated four types of $Ti(O_2^{-\bullet})$ species, A′, A, B, and C. Only species B was detected in the TiMCM-41 + UHP system. The *g*-values of the various $Ti(O_2^{-\bullet})$ species differ mainly in their g_z parameter (Table 1). At least six different $Ti(O_2^{-\bullet})$ species (A, A′, A″, B, B′, and C) were detected in Pd(*n*)–TS-1 (Figs. 3 and 4). The Ti sites adjacent to Pd ions are magnetically different than the other Ti ions, accounting for the greater variety of $Ti(O_2^{-\bullet})$

Table 1
EPR parameters of the oxo–titanium(IV) species

System	Species	g_z	g_y	g_x	Δ (cm^{-1})
TS-1 + HP	A	2.0264	2.0090	2.0023	11203
	B	2.0238	2.0090	2.0023	12558
TiMCM-41 + HP	B	2.0244	2.0095	2.0031	12217
Pd(2)–TS-1 + HP	A′	2.0309	2.0100	2.0350	9440
	A	2.0276	2.0100	2.0350	10672
	A″	2.0265	2.0100	2.0350	11157
	B′	2.0255	2.0100	2.0350	11638
	B	2.0245	2.0100	2.0350	12162
	C	2.0220	2.0100	2.0350	13705
TS-1 + UHP	A′	2.0300	2.0101	2.0035	9747
	A	2.0275	2.0101	2.0035	10715
	B	2.0242	2.0101	2.0035	12329
	C	2.0206	2.0101	2.0035	14754
TiMCM-41 + UHP	B	2.0232	2.0096	2.0046	12919
TS-1 + H_2 + O_2	A	2.0265	2.0080	2.0010	11157
	Ti^{3+}	1.930	1.956	1.956	
Pd(2)–TS-1 + H_2 + O_2	A′	2.0340	2.0092	2.0022	8517
	A″	2.0295	2.0092	2.0022	9926
	B	2.0241	2.0092	2.0022	12385
	Ti^{3+}	1.928	1.953	1.953	
Pt(0.015)–TS-1 + H_2 + O_2	A′	2.0300	2.0080	2.0012	9747
	A‴	2.0295	2.0080	2.0012	9890
	B	2.0241	2.0080	2.0012	12385
	Ti^{3+}	1.931	1.955	1.955	

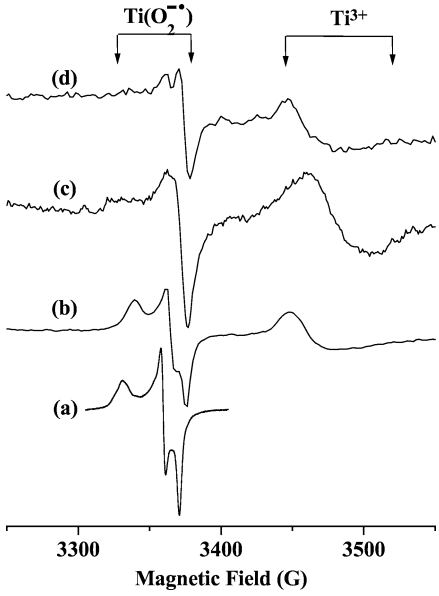

Fig. 3. EPR spectra of $Ti(O_2^{-\bullet})$ and Ti^{3+} ions at 80 K. (a) Pd(2)–TS-1 + H_2O_2, (b) Pt(0.015)–TS-1 + H_2 + O_2 (treated at 673 K), (c) Pd(2)–TS-1 + H_2 + O_2 (treated at 323 K), and (d) TS-1 + H_2 + O_2 (treated at 673 K). For clarity curves c and d are shown at four and five times the actual gain. Spectral regions corresponding to $Ti(O_2^{-\bullet})$ and Ti^{3+} ions are marked.

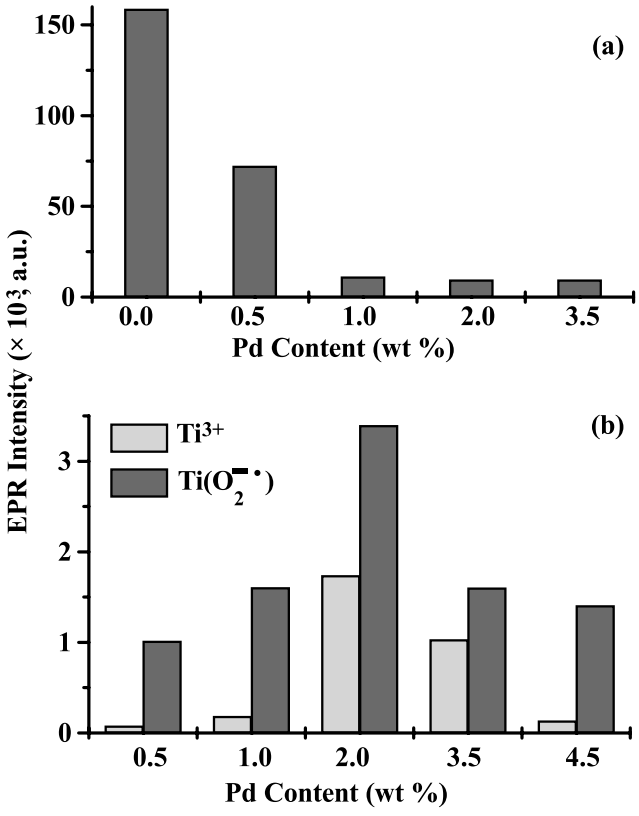

Fig. 4. (a) EPR spectral intensity of $Ti(O_2^{-\bullet})$ ions as a function of Pd content in Pd(n)–TS-1 samples on reaction with H_2O_2. (b) EPR spectral intensity of Ti^{3+} and $Ti(O_2^{-\bullet})$ ions as a function of Pd content in Pd(n)–TS-1 reacted with H_2 + O_2.

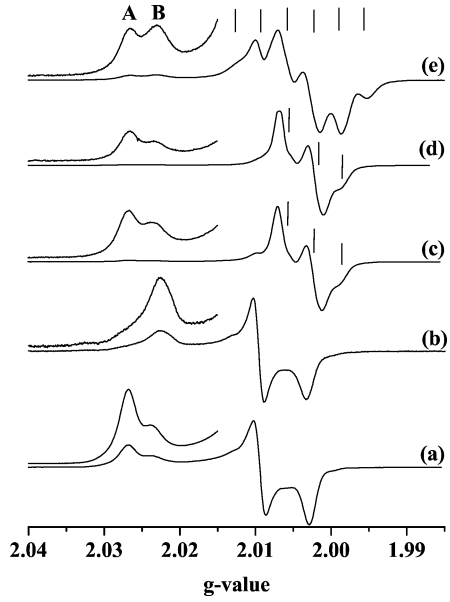

Fig. 5. EPR spectra at 180 K of TS-1 + H_2O_2 in the presence of substrate. (a) No substrate, (b) allylalcohol, (c) phenol, (d) benzene, and (e) toluene. Signals indicated by the vertical lines are due to the substrate-based radicals formed during the oxidation reaction.

species. Control experiments on silicalite-1 and Si–MCM-41 samples reacted with HP did not show signals in EPR; they were seen only in the Ti-containing samples. In addition, the intensity of the reductive oxygen signals increased linearly with Ti content in the silicalite samples (Si/Ti = 80, 60, and 30). These blank experiments confirm that the EPR signals in the present case arise only from the Ti sites.

In the absence of H_2, exposure of TS-1, TiMCM-41, Pd–TS-1, or Pt–TS-1 to O_2 alone does not generate the superoxide species. When Pd(Pt)–TS-1 samples are contacted with H_2 + O_2, Ti^{4+} is reduced to Ti^{3+} by H_2 (Fig. 3). The Ti^{3+} ion generates $Ti(O_2^{-\bullet})$ species on interaction with O_2. The EPR signals due to Ti^{3+} and $Ti(O_2^{-\bullet})$ (Fig. 3, Table 1) are well separated and can be differentiated. This reduction and reoxidation of Ti ions, which requires 673 K or above in TS-1, is facilitated by Pd or Pt even at 323 K (Fig. 3, compare traces a and c). The superoxo species generated are more of A and A′ type (Fig. 3, Table 1). The extent of Ti reduction and $Ti(O_2^{-\bullet})$ formation depends on the Pd content, with the concentration of the paramagnetic Ti–oxo species reaching maximal values of 2% (wt) Pd (Fig. 4).

3.3. Catalytic oxidation over TS-1: in situ EPR study

TS-1 (40 mg) in an EPR cell was reacted with 50% aqueous H_2O_2 (0.1 ml). On further contact with the substrate (allyl alcohol, benzene, phenol, or toluene; 0.1 ml) the intensity of the $Ti(O_2^{-\bullet})$ species decreased. In the absence of the substrate the intensity of type A species in TS-1 was more than that of type B (Fig. 2). On adding allyl alcohol, the reaction was highly exothermic and the concentration of the type A species decreased faster than that of type B, indicat-

Table 2
Catalytic activity data in the expoxidation of allyl alcohol over TS-1 and Pd(n)–TS-1 catalysts[a]

Catalyst	Oxidant	TOF[b]	H_2O_2 efficiency (%)	Conversion (wt%)	Epoxide selectivity (wt%)
TS-1	H_2O_2	15.3	42.8	77.0	96.1
Pd(0.5)–TS-1	H_2O_2	12.3	34.2	61.5	95.6
Pd(2)–TS-1	H_2O_2	10.5	28.8	51.7	90.4
Pd(3.5)–TS-1	H_2O_2	7.6	20.7	37.1	82.8
Pd(4.5)–TS-1	H_2O_2	6.2	16.7	30.0	74.0
Pd(2)–TS-1	$H_2 + O_2$	2.1	–	10.5	99.0

[a] Reaction medium: catalyst (100 mg) + allyl alcohol (0.5 g) + acetone (10 g) + H_2O_2 (50%, 0.9 ml); temperature = 333 K; run time = 8 h.
[b] Turnover frequency (TOF) = moles of allyl alcohol converted per mole of Ti per hour.

ing the faster consumption of the former. The spectrum, after 10 min of the reaction at 318 K, contained only the unreacted species B. When the TS-1 + HP slurry was contacted with toluene, benzene, or phenol, the color of the solution changed initially to orange and then dark blackish-green. In the case of phenol or benzene the initially generated species B was consumed faster than A (Fig. 5, curves b and c). Species B are, apparently, more active than A in ring hydroxylation reactions. In the case of toluene oxidation, the intensity of both A and B are altered on addition of the substrate (curve d), revealing that both species A and B are probably involved in the oxidation of toluene. Comparison of the toluene results with those of phenol/benzene suggests that while species B is involved in ring hydroxylations, species A may be involved in the side chain oxidation. In reactions with benzene/phenol/toluene, at least two types of radicals were formed (Fig. 5; denoted by vertical lines). Their identity is not clear at present. These radicals were not formed in the presence of allyl alcohol. The catalytic activity data using ($H_2 + O_2$) as the oxidant over Pd(2)–TS-1 (Table 2) also confirm the correlation between the epoxidation selectivity and the concentration of type A species. Higher epoxide selectivities were observed also in the TS-1 + UHP system [20], where species A′ was predominant. Our in situ studies suggest that different oxo species lead to different products.

3.4. DRUV–visible spectroscopy

On reaction with HP or UHP, an asymmetric, broad band, which can be deconvoluted into two bands (I and II), was observed (Fig. 6). Bands I and II are attributed to the charge transfer transitions associated with Ti(IV)–superoxo ($Ti(O_2^{-\bullet})$) and Ti(IV)–hydroperoxo (Ti(OOH)) species, respectively. The position and relative intensity of these bands are different in HP– and UHP–TS-1 systems and in Pd-containing samples. For TS-1 + HP, these bands occur at 360 and 405 nm. For Pd(2)–TS-1 + HP, they occur at 339 and 387 nm and for TS-1 + UHP at 345 and 408 nm. The bandwidth at half maximum of I and II, in TS-1 + HP/UHP

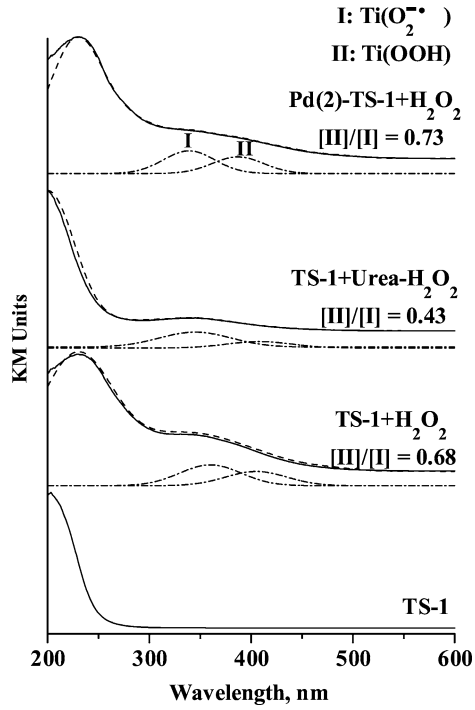

Fig. 6. DRUV–visible spectra of TS-1, TS-1 + H_2O_2, TS-1 + urea–H_2O_2, and Pd(2)–TS-1 + H_2O_2. Bands due to superoxo (I) and hydroperoxo (II) species are marked. Experimental (—), simulated (– – –), and deconvoluted oxo–titanium bands (–·–·–).

systems, is 70 and 75 nm, respectively, and it is 60 nm in Pd(2)–TS-1 + HP. The intensity ratio [II/I] decreases in the following order: Pd(2)–TS-1 + HP (0.73) > TS-1 + HP (0.68) > TS-1 + UHP (0.43). In TiMCM-41 + HP these bands overlap with the TiMCM-41 bands. These results suggest that UHP generates predominantly the superoxo species while HP stabilizes the hydroperoxo species. Conversion energy for hydropero–superoxo transformation was estimated, from the DRUV–visible band positions of II and I, in TS-1 + HP, Pd(2)–TS-1 + HP, and TS-1 + UHP to be 9.7, 11.5, and 14.1 kcal/mol, respectively. This energy correlates with the energy of the reaction: Ti–OOH → $Ti(O_2^{-\bullet}) + H^+$ and supports the assignments of the UV–visible bands. To the best of our knowledge, this is the first report on the identification and estimation of Ti(IV)–hydroperoxo and –superoxo species by DRUV–visible spectroscopy. Most of the earlier work [21] had reported only a broad unresolved band in the region 300–500 nm. The hydroperoxo– and superoxo–titanium species are independently estimated from EPR and found to be 45 and 55%, respectively, at 80 K. Thus, the Ti(OOH)/$Ti(O_2^{-\bullet})$ ratio is found to be 0.82 at 80 K. At 298 K this ratio is lower. The comparative value from DRUV–visible experiments, at 298 K for TS-1 + HP, is 0.66. This independent EPR estimation of the concentration of the oxo–titanium also supports our assignments of the DRUV–visible bands to the Ti–hydroperoxo and –superoxo species.

3.5. Catalytic activity of Pd(n)–TS-1 in the epoxidation of allyl alcohol

Allyl alcohol conversions of 77% and epoxide selectivities of 96% were obtained over TS-1 catalysts at 333 K. Over Pd(n)–TS-1 catalysts, the conversion and selectivity decreased with increasing Pd content (Table 2), consistent with the lower Ti($O_2^{-\bullet}$) signal intensities at higher Pd content (Fig. 4a). Pd catalyzes the decomposition H_2O_2 into H_2O and O_2 and leads to lowered H_2O_2 efficiency for epoxidation. In addition to epoxidation, the acid-catalyzed condensation of epoxide with solvent acetone also takes place over the Pd-containing TS-1 catalysts.

Tentative structures of A, B, and C, arising from the tetrahedral TiO_4 unit on interaction with H_2O_2, are shown in Fig. 7. Species A arises from the substitutional tetrahedral Ti sites and B and C arise from the defect sites. The free $O_2^{-\bullet}$ radical with a $^2\Pi$ ground state has a $(1\sigma_g)^2(1\sigma_u)^2(2\sigma_g)^2(2\sigma_u)^2(3\sigma_g)^2(1\pi_u)^4(1\pi_g)^3$ electronic configuration. Interaction with Ti removes the degeneracy of the HOMO π_g into π_g^x and π_g^y orbitals with an energy gap of Δ. Neglecting the second-order terms, the g-value expressions (when $\lambda < \Delta \ll E$) are written as [22] $g_z = g_e + 2\lambda/\Delta$, $g_y = g_e + 2\lambda/E$, and $g_x \approx g_e$, where $g_e = 2.0023$, λ is the spin orbit coupling constant (135 cm^{-1} for oxygen), and E is the energy separation between $3\sigma_g$ and $1\pi_g^x$ orbitals. The g_z-value of the superoxo anion is sensitive to the oxidation state, coordinating number, and local geometry of the cation to which it is coordinated. Ti–($O_2^{-\bullet}$) distances also influences the g_z parameter. The stronger the Ti–O bond, the lower the g_z-value of the superoxo anion. Using the above expressions and the experimental g_z-value, we estimated the separation between the π_g^x and π_g^y orbitals (Δ) (Table 1). The g_z-values of different Ti($O_2^{-\bullet}$) species decrease in the order A type (A, A′, and A″) > B type (B, B′) > C type. The Δ values vary in the reverse order. Hence, the strength of the Ti–O bond increases in the order A type < B type < C type. The O–O bond strength follows the reverse order. The type A species is, probably, the active intermediate in epoxidations while B and C lead to nonselective oxidations (Fig. 7). TS-1 generates type A species in greater abundance than does TiMCM-41, which generates mostly the type B species from H_2O_2. The greater epoxidation selectivity of TS-1 (compared to TiMCM-41) probably arises from this crucial difference. The present work also provides, for the first time, experimental evidence for the formation of reactive oxo species in the interaction of $H_2 + O_2$ over Pd(n)–TS-1 catalysts. *Even though similar oxo species are formed over all the titanosilicates in the presence of either H_2O_2 or $H_2 + O_2$, their relative concentration determines the catalytic activity and selectivity*. A schematic representation of the possible role of Pd is shown in Fig. 8.

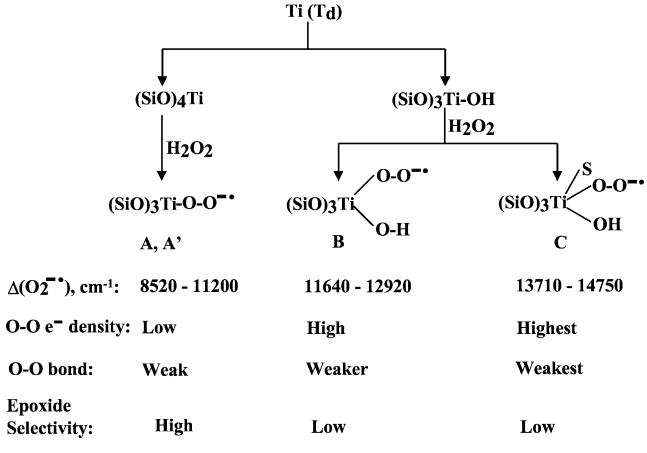

Fig. 7. Schematic diagram of different Ti($O_2^{-\bullet}$) species generated by H_2O_2.

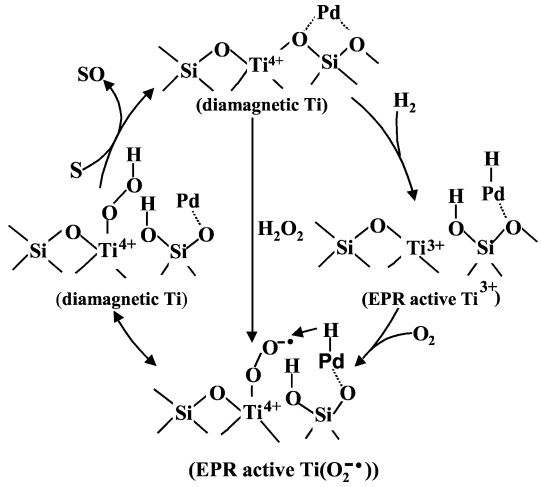

Fig. 8. Role of Pd in the in situ generation of H_2O_2 from $H_2 + O_2$ over Pd(n)–TS-1 catalysts. S denotes the substrate and SO the oxygenated product.

4. Conclusions

Interaction of titanoslilicates (TS-1, TiMCM-41, and Pd(n)–TS-1) with H_2O_2, urea–H_2O_2, and ($H_2 + O_2$) generates reactive Ti(IV)–superoxo and hydroperoxo/peroxo species. These could be identified and quantified, for the first time, by DRUV–visible and EPR spectroscopies. Two types of Ti(IV)–superoxo species, A and B (A being preponderant), were detected in TS-1; TiMCM-41 contained mainly species B. Pd–TS-1 generated six types of Ti–oxo species. Epoxidation selectivities were correlated to the relative concentration of these various oxo species during the reaction. Type A species were mainly responsible for epoxidation of olefins while aromatic ring hydroxylations were promoted by type B species. The greater selectivity of TS-1 (over TiMCM-41) in epoxidations is, probably, due to the formation of type A species in greater quantities over the former. Pd enhances the reducibility of Ti^{4+} ions to Ti^{3+} by H_2 at lower temperatures (323 K), thereby facilitating the formation of similar reactive Ti–oxo species from $H_2 + O_2$.

References

[1] B. Notari, Adv. Catal. 41 (1996) 253, and the references therein.
[2] G.N. Vayssilov, Catal. Rev.–Sci. Eng. 39 (1997) 209, and the references therein.
[3] G. Tozzola, M.A. Mantegazza, G. Ranghino, G. Petrini, S. Bordiga, G. Ricchiardi, C. Lamberti, R. Zulian, A. Zecchina, J. Catal. 179 (1998) 64.
[4] G. Sankar, J.M. Thomas, C.R.A. Catlow, C.M. Barker, D. Gleeson, N. Kaltsoyannis, J. Phys. Chem. B 105 (2001) 9028.
[5] E. Karlsen, K. Schoffel, Catal. Today 32 (1996) 107.
[6] A. Corma, M.T. Navarro, J. Perez Pariente, J. Chem. Soc. Chem. Commun. (1994) 147.
[7] P.T. Tanew, M. Chibwe, T.J. Pinnavaia, Nature 368 (1994) 321.
[8] J.D. Jewson, C.A. Jones, R.M. Dessau, PCT Int. Appl. WO 2001062380 A1, 2001.
[9] R. Meiers, U. Dingerdissen, W.F. Hölderich, J. Catal. 176 (1998) 376.
[10] R. Meiers, W.F. Hölderich, Catal. Lett. 59 (1999) 161.
[11] G. Jenzer, T. Mallat, M. Maciejewski, F. Eigenmann, A. Baiker, Appl. Catal. A 208 (2001) 125.
[12] E.E. Stangland, K.B. Stavens, R.P. Andres, W.N. Delgass, J. Catal. 191 (2000) 332.
[13] C. Qi, T. Akita, M. Okumura, M. Haruta, Appl. Catal. A 218 (2001) 81.
[14] T.A. Nijhuis, B.J. Huizinga, M. Makkee, J.A. Moulijn, Ind. Eng. Chem. Res. 38 (1999) 884.
[15] K. Chaudhari, D. Srinivas, P. Ratnasamy, J. Catal. 203 (2001) 25.
[16] A. Thangaraj, R. Kumar, S.P. Mirajkar, P. Ratnasamy, J. Catal. 130 (1991) 1.
[17] R. Bal, K. Chaudhari, D. Srinivas, S. Sivasanker, P. Ratnasamy, J. Mol. Catal. A 162 (2000) 199.
[18] A. Tuel, J. Diab, P. Gelin, M. Dufaux, J.-F. Dutel, Y. Ben Taarit, J. Mol. Catal. A: Chem. 63 (1990) 95.
[19] F. Geobaldo, S. Bordiga, A. Zecchina, E. Giamello, G. Leofanti, E. Petrini, Catal. Lett. 16 (1992) 109.
[20] S.C. Laha, R. Kumar, J. Catal. 204 (2001) 64.
[21] J.F. Bengoa, N.G. Gallegos, S.G. Marchetti, A.M. Alvarez, M.V. Cagnoli, A.A. Yeramian, Microporous Mesoporous Mater. 24 (1998) 163.
[22] M. Che, A.J. Tench, Adv. Catal. 32 (1983) 1.